Insights on Lateral Gravity Wave Propagation in the Extratropical Stratosphere from 44 Years of ERA5 Data

Aman Gupta[1], Aditi Sheshadri[1], M. Joan Alexander[2], and Thomas Birner[3,4]

[1]Doerr School of Sustainability, Stanford University, Stanford, California, USA
[2]NorthWest Research Associates, Boulder, Colorado, USA
[3]Meteorological Institute, Ludwig Maximilians Universität, Munich, Germany
[4]Institut für Physik der Atmosphäre, Deutsches Zentrum für Luft und Raumfahrt (DLR), Oberpfaffenhofen, Germany

Key Points:

- Climatology of lateral fluxes from ERA5 shows substantial lateral propagation of gravity waves in both hemispheres
- Climatological contribution of lateral GW fluxes towards zonal mean forcing is the same order of magnitude as that from vertical fluxes
- Abrupt changes in GW forcing in the upper stratosphere around sudden stratospheric warmings can last up to 20 days following the event

Corresponding author: Aman Gupta, ag4680@stanford.edu

Abstract

The study presents (a) a 44-year wintertime climatology of resolved gravity wave (GW) fluxes and associated zonal forcing in the extratropical stratosphere using ERA5, and (b) their composite evolution around gradual (final warming) and abrupt (sudden warming) transitions in the wintertime circulation. The connection between transformed Eulerian mean (TEM) equations and the linear GW pseudomomentum is leveraged to provide a glimpse of the importance of GW lateral propagation toward driving the wintertime stratospheric circulation by analyzing the relative contribution of the vertical vs. meridional flux convergence. The relative contribution from lateral propagation is found to be notable, especially in the Austral winter stratosphere where lateral (vertical) momentum flux convergence provides a peak climatological forcing of up to –0.5 (–3.5) m/s/day around 60°S at 40-45 km altitude. Prominent lateral propagation in the wintertime midlatitudes also contributes to the formation of a belt of GW activity in both hemispheres.

Plain Language Summary

Internal gravity waves (GWs) exhibit both vertical and horizontal (lateral) propagation in the atmosphere, influenced by the background shear of the flow that supports them. GW model parameterizations, however, represent them in climate models assuming strict vertical propagation. This modeling assumption can have implications for modeled large-scale stratospheric circulation and variability. This study uses ERA5 reanalysis to produce the climatological distribution of resolved GW momentum fluxes and forcing in the stratosphere, and their composite evolution around prominent patterns of extratropical stratospheric variability like sudden stratospheric warmings (SSWs) and springtime final warmings (FWs). The climatology reveals that lateral propagation leads to the formation of a belt of rich GW activity in the upper winter stratosphere, which is otherwise localized over orographic hotspots in the lower stratosphere. The resolved forcing due to lateral GW propagation is found to be roughly the same order of magnitude as resolved forcing due to vertical fluxes, underlining the importance of lateral propagation for future GW parameterizations. Strikingly different GW forcing profiles are evident before vs. after SSWs and FWs, highlighting the strong two-way connection between GWs and the stratospheric mean flow.

1 Introduction

Gravity waves (GWs) dynamically couple the different layers of the atmosphere and are among the key drivers of the meridional overturning circulation in the middle atmosphere (Fritts & Alexander, 2003; Achatz et al., 2023). They provide a zeroth-order contribution towards driving the pole-to-pole mesospheric circulation (Holton, 1982; Fritts & Alexander, 2003; Becker, 2012). In the stratosphere, they influence the quasi-biennial oscillation (QBO) of tropical winds (Giorgetta et al., 2002), and the springtime breakdown of the Antarctic polar vortex (Gupta et al., 2021). GWs can also contribute to rapid breakdowns of the wintertime polar vortex, i.e., sudden stratospheric warmings (Albers & Birner, 2014; Song et al., 2020), eventually influencing tropospheric storm tracks (Kidston et al., 2015; Domeisen & Butler, 2020).

Atmospheric GWs are generated by a myriad of sources (e.g., convection, orography, jets, and fronts) and manifest over spatial scales ranging from $\mathcal{O}(10)$ km to $\mathcal{O}(1000)$ km, and evolve over temporal scales ranging from ∼5 minutes to over a day (Fritts & Alexander, 2003). The true impact of GWs on the stratospheric circulation, and its evolution under a changing climate, is not fully understood because of limited global observations, inadequately parameterized representation in stratosphere-resolving climate models, and computationally prohibitive costs of running GW-resolving high-resolution models (Kim et al., 2003; Alexander et al., 2010; Geller et al., 2013; Plougonven et al., 2020).

Current GW parameterizations assume strict vertical propagation and therefore, only approximate their vertical momentum transport, i.e., they ignore their lateral (zonal and meridional) propagation. In this approximation, the net forcing due to dissipating GWs is typically estimated using the covariances ($\overline{u'\omega'}, \overline{v'\omega'}$) and their absolute magnitude $\sqrt{\overline{u'\omega'}^2 + \overline{v'\omega'}^2}$ (e.g., Wei et al. (2022)). Here u, v, and ω are the zonal, meridional, and pressure velocities, and the primes denote their deviation from the background flow. The covariances are approximated from GW-resolving models and observations, and the estimates are frequently used to tune subgrid-scale GW parameterizations for coarser climate models.

Recent analyses (Kruse et al., 2022; Procházková et al., 2023) quantified the contribution from lateral fluxes (in addition to the usual vertical fluxes) using a suite of mesoscale-resolving numerical weather prediction models over the Drake Passage. The studies found notable forcing over a 10-day period from lateral flux terms. The importance of these terms is further corroborated by Sun et al. (2023) who extracted and compared horizontal GW fluxes using three different techniques. Yet, these lateral fluxes are universally ignored by model parameterizations of GWs. Representing lateral propagation in parameterizations would be expected to ensure a more accurate representation of GWs in climate models (Sato et al., 2009; Alexander & Grimsdell, 2013; Sato et al., 2012; Plougonven et al., 2020; Polichtchouk & Scott, 2020; Pahlavan et al., 2023; Gupta et al., 2024).

This study presents a multidecadal climatology of both the vertical and lateral GW fluxes and provides a glimpse into their contribution to the stratospheric circulation, using ERA5. The contribution of the lateral fluxes towards forcing the zonal winds in the stratosphere is evaluated against the forcing provided solely by the vertical flux, $\overline{u'\omega'}$. This is done by (a) producing a 44-year (1979-2022) DJF and JJA climatology of the vertical and horizontal transport of GW pseudomomentum during peak winters, and (b) producing a composite evolution of these terms around sudden stratospheric warmings (SSWs) in the Northern Hemisphere and the springtime final warmings (FWs) in the Southern Hemisphere.

2 Background

For non-dissipating gravity waves, the vertical flux of zonal pseudomomentum can be related to the Reynolds fluxes, in pressure coordinates, as (Fritts & Alexander, 2003; Gill, 1982):

$$F_{zx} = \frac{-1}{g} c_{gz} \frac{E}{\hat{\omega}} k = \frac{-1}{g} \left(1 - \frac{f^2}{\hat{\omega}^2}\right) \overline{u'\omega'} \tag{1}$$

where c_{gz} is the vertical group velocity, $\hat{\omega}$ is the intrinsic frequency, k is the zonal wavenumber, E is the kinetic + potential GW energy density, f is the Coriolis parameter, u is the zonal wind, ω is the vertical velocity in pressure coordinates, and overbar denotes averaging over single/multiple wave cycles (even a zonal mean).

Likewise, the meridional flux of zonal pseudomomentum relates to the Reynolds fluxes as:

$$F_{yx} = c_{gy} \frac{E}{\hat{\omega}} k = \overline{u'v'} \tag{2}$$

where c_{gy} is the meridional group velocity of the GW.

Now, the zonal mean zonal wind evolution, in Transformed Eulerian Mean (TEM) form, is expressed as (Andrews et al., 1987):

$$\overline{u}_t = \left(f - \frac{1}{R\cos\phi}(\overline{u}\cos\phi)_\phi\right)\overline{v}^* - \overline{u}_p\overline{\omega}^* + \underbrace{\frac{1}{R\cos\phi}\vec{\nabla}\cdot\vec{F}}_{\text{EPFD}} + \overline{X} \tag{3}$$

where ϕ is latitude, p is pressure, t is time, the overbar denotes zonal mean along constant pressure surfaces, subscripts denote partial derivatives, $\overline{u}$ is the zonal mean zonal wind, $\overline{v}^*$ and $\overline{\omega}^*$ are respectively the residual meridional and vertical velocities, $\overline{X}$ is the zonal mean parameterized GW forcing, R is the radius of the earth, and $\vec{F}$ is the Eliassen-Palm (EP)-flux vector:

$$\vec{F} = \left(F^{(\phi)}, F^{(p)}\right) = R\cos\phi\left(-\overline{u'v'} + \overline{u}_p\frac{\overline{v'\theta'}}{\overline{\theta}_p}, \left(f - \frac{1}{R\cos\phi}(\overline{u}\cos\phi)_\phi\right)\frac{\overline{v'\theta'}}{\overline{\theta}_p} - \overline{u'\omega'}\right) \quad (4)$$

where θ is the potential temperature.

The r.h.s. covariances in Eqn 4, when computed for large-scale (small-scale) perturbations, represent the total meridional and vertical momentum flux due to planetary waves (gravity waves). The total vertical EP-Flux in Eqn 4 equals the total vertical flux of zonal pseudomomentum in Eqn 1. Likewise, the total meridional EP-Flux in Eqn 4 equals the total meridional flux of zonal pseudomomentum in Eqn 2. Thus, the EP-Flux vector, computed for small-scale perturbations, fully estimates the net meridional and vertical GW momentum flux. The meridional component, which climate model parameterizations ignore, quantifies the lateral propagation of momentum by GWs, and as shown later, can provide notable contributions to mean flow forcing.

The divergence of the wave-momentum fluxes, represented by the divergence of the EP-Flux vector, then, represents the total forcing applied by the dissipating planetary waves (gravity waves) on the background flow. The EP-Flux divergence (EPFD) can be expressed as:

$$\frac{1}{R\cos\phi}\vec{\nabla}\cdot\vec{F} = \frac{1}{R\cos\phi}\left(\frac{1}{R\cos\phi}\left(F^{(\phi)}\cos\phi\right)_\phi + F_p^{(p)}\right) \quad (5)$$

The total EPFD comprises contributions from four terms:

i. meridional convergence of momentum: $\frac{-1}{R\cos^2\phi}\left(\overline{u'v'}\cos^2\phi\right)_\phi$
ii. meridional heat convergence: $\frac{1}{R\cos^2\phi}\left(\overline{u}_p\frac{\overline{v'\theta'}}{\overline{\theta}_p}\cos^2\phi\right)_\phi$
iii. vertical heat convergence: $\left(\left[f - \frac{(\overline{u}\cos\phi)_\phi}{R\cos\phi}\right]\frac{\overline{v'\theta'}}{\overline{\theta}_p}\right)_p$
iv. vertical convergence of momentum: $-\overline{u'\omega'}_p$

This means both vertical and meridional transport of GW pseudomomentum contribute to the acceleration/deceleration of the zonal mean zonal wind. In the following sections, we refer to these four forcing terms as the $\overline{u'v'}_\phi$, $\overline{v'\theta'}_\phi$, $\overline{v'\theta'}_p$, and the $\overline{u'\omega'}_p$ terms respectively.

3 Computing the Resolved GW Forcing in ERA5

The GW fluxes and forcing were computed using the hourly reanalysis, ERA5 (Hersbach et al., 2020), from the European Centre for Medium-Range Weather Forecasting (ECMWF) on pressure levels over 1979-2022. The data is publicly available at a 0.25°×0.25° horizontal resolution and 37 vertical (pressure) levels from 1 hPa to 1000 hPa. The small-scale perturbations of the fields were computed by removing the first 21 total wavenumbers from the full fields (u, v, ω, and T), and then tapering the wavenumbers 21 to 42 (scales 500-1000 km in the midlatitudes) using a Gaussian tapering in spectral space with a half-width of ∼5.5. This means the spectral coefficients were almost completely damped for wavenumber 22, damped by a factor of ∼2 for wavenumber 35, almost fully retained for wavenumber 40, and fully retained for wavenumbers 42 and above. The gradual tapering leads to a smoother separation between the large- and small-scales. The filtered variables were then multiplied to compute the covariances.

Accounting for grid-scale hyperdiffusion and other numerical effects, ERA5 still resolves GWs with wavelengths 200 km and longer. Stratospheric and mesospheric sponges are applied at pressures less than 10 hPa and 1hPa respectively, to numerically "absorb" vertically propagating GWs.

3.1 Defining Sudden Stratospheric Warmings (SSWs)

An SSW is broadly defined as an extreme, abrupt deceleration of the wintertime stratospheric polar vortex within a short period of 5-7 days. Major SSWs are SSW events where the deceleration of the vortex is so strong that it leads to a total, albeit short-term, westerly-to-easterly reversal of the polar night jet (Butler et al., 2017; Baldwin et al., 2021). To create composites around SSWs, we identify a major SSW as the date when the abrupt wind reversal first occurs at 60°N and 10 hPa. Over the 1979-2023 DJF period, 30 such SSW events have been identified in the Northern Hemisphere (Table S1).

3.2 Defining Final Warmings (FWs)

FWs in the Austral stratosphere are defined as the springtime westerly-to-easterly transition of the zonal mean zonal wind. In this study, we identify the FW date as the first day following Austral winters when the zonal mean zonal wind at 60°S and 10 hPa turns easterly. All FW composites are produced around this date (Table S1).

4 44-year Climatology of GW Forcing in the Extratropical Stratosphere

The climatology of zonal mean GW forcing is shown in Figure 1. In both hemispheres, the $\overline{u'\omega'}_p$ term provides the strongest contribution, providing an average resolved forcing of up to –2 m/s/day in the Northern Hemisphere (DJF) and up to –4 m/s/day in the Southern Hemisphere (JJA) (Figure 1a). Most GW dissipation occurs above 10 hPa, and spans the midlatitudes in both hemispheres. Downward protrusions in the JJA forcing pattern, between 3-10 hPa, at 45°S and 75°S respectively show contributions from GWs excited over the Andes and Antarctic peninsula. The direction of flux propagation, shown by the small-scale EP-Flux vectors (Figure 1a), shows upward and poleward propagation of GWs, and focusing of momentum towards the polar night jet.

The $\overline{u'v'}_\phi$ term provides the second strongest zonal mean forcing (Figure 1b) in the upper stratosphere. The forcing is strongest in the Southern Hemisphere midlatitudes, with a net zonal acceleration between 40-50°S, and a net zonal deceleration of up to – 0.5 m/s/day poleward of 50°S. Between 10-30 hPa, the JJA forcing from the $\overline{u'\omega'}_p$ and $\overline{u'v'}_\phi$ terms are, in fact, equally strong. The Northern Hemispheric forcing is weaker, on average, due to a weaker vortex perturbed with frequent warming events. For strong vortex days, the DJF deceleration is at least double the climatological average, and therefore, similar in strength to the JJA forcing (Figure S1). The vertical momentum convergence provides a bulk of the forcing, but the notable contribution from lateral flux convergence highlights the prominence of lateral propagation of GWs in the upper stratosphere.

The vertical heat flux convergence provides strong forcing between 30°-50° latitudes, but an order of magnitude weaker forcing in the upper stratosphere (Figure 1c vs. 1a). This indicates strong contributions from resolved inertio-gravity waves likely due to geostrophic adjustment around the midlatitude jet core (Plougonven & Zhang, 2014).

The horizontal maps of the DJF and JJA mean $u'\omega'$ and $u'v'$ are illustrated in Figure 2. In the lower stratosphere, $u'\omega'$ is mostly localized near orographic hotspots including the Rocky Mountains, Himalayas, Scandinavian Mountains, and European Alps (Figure 2a,b; green). In the middle stratosphere, the flux increasingly spreads horizontally beyond the mountain ranges (Figure 2a,b; blue) to the extent that in the upper stratosphere, the fluxes form almost a global belt of GW activity spanning at least half the latitudinal circle (Figure 2a,b; color). The belt spans from ∼60°W to ∼180°E.

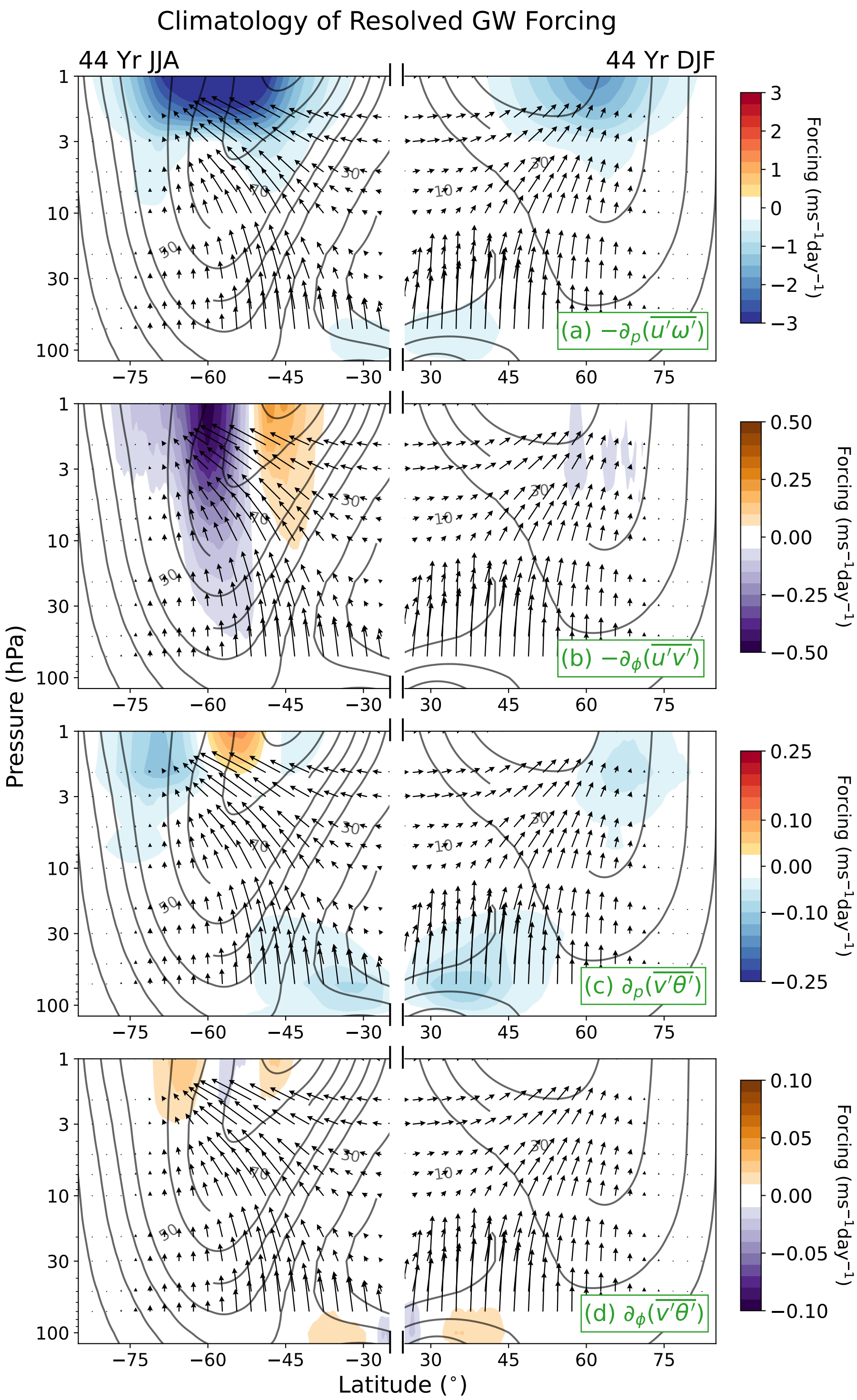

Figure 1. 44-year (1979-2022) JJA and DJF climatology of the four forcing terms (m/s/day) in Eqn 5 forming the total resolved small-scale forcing. The black curves and black arrows show the zonal mean zonal wind (m/s) and the small-scale EP-Flux respectively.

The hotspots in both hemispheres identified in ERA5 match well with those identified from AIRS temperature data (Hindley et al., 2020). The hotspots contributing most to the belt in the Northern Hemisphere include Newfoundland and Long-Range mountains in Canada, southeastern Greenland, the British Isles, Scandinavian mountain ridge, the Italian Alps, the Ural mountains in Eurasia, Altay-Sayan and the Greater Khingan mountains in Central and East Asia (Figure 2a). Interestingly, the strong fluxes over the Rocky Mountains, the Himalayas, and the Japanese islands do not contribute to the upper stratospheric belt as they dissipate in the lower stratosphere.

Similarly, in the Southern Hemisphere, the most notable contributions to the GW activity belt in the upper stratosphere are found over the Andes, the Antarctic peninsula, and the Southern Ocean with some contributions from New Zealand (Figure 2b; color). In the lower stratosphere, most of the GW activity is localized over these two mountain ranges (Figure 2b; green). As the GWs propagate vertically (and laterally), the GW activity in the middle stratosphere steadily spreads wider to regions downstream of the Andes, including most parts of the Southern Ocean (Figure 2b; blue curve).

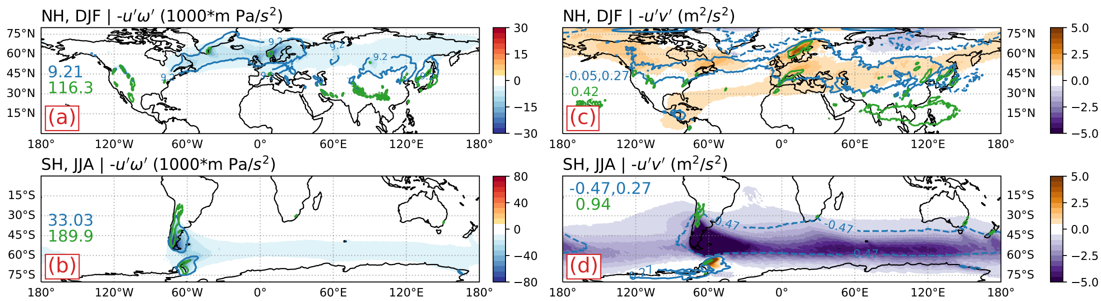

Figure 2. The map of the 44-year averaged (a)-(b) vertical flux ($u'\omega'$) and (c)-(d) lateral flux ($u'v'$), at 2 hPa altitude. Superimposed green and blue curves show the 10$^{\text{th}}$-percentile envelope of the respective flux in the lower stratosphere (100 hPa) and the middle stratosphere (20 hPa) respectively. The values for the solid (positive) and dashed (negative) blue and green curves are specified in the respective figures, with units as specified in the subplot titles.

Lateral propagation is evident in both hemispheres, more so around prominent mountain ranges. The horizontal flux, $\overline{u'v'}$, in the Northern Hemisphere maximizes over the Canadian Rockies, Appalachian Mountains, the Scandinavian mountains, and the European Alps, and indicates a predominantly poleward transport of zonal momentum (Figure 2c). Strong meridional convergence over these spots contributes the most to the zonal mean forcing provided by lateral fluxes.

In the Southern Hemisphere (Figure 2d), strongly negative $\overline{u'v'}$ indicates strong poleward propagation of momentum by GWs. Negative (poleward) fluxes over and downstream of the Andes and positive (equatorward) fluxes around the Antarctic peninsula indicate momentum convergence over the Drake Passage. Though the fluxes maximize around these topographies, a streak of lateral fluxes spans the whole latitudinal circle. Using the 7-km GEOS Nature run, Holt et al. (2017) identified midlatitude-to-subtropical convection near 100 hPa as a primary source of GWs in the Southern Hemisphere. These strong but interspersed sources could form key contributions to the upper stratospheric streak.

5 Composite Evolution of Vertical and Lateral GW Fluxes

5.1 Evolution around SSWs

To analyze the GW forcing evolution during abrupt dynamical changes in the stratosphere, we assess the composite evolution of the resolved forcing around 30 major SSWs over 1979-2023 (Figure 3). On average, the vortex decelerates by 35-40 m/s over 20 days leading to the SSWs, the deceleration being much stronger for the 7 days prior to wind reversal (Figure 3a).

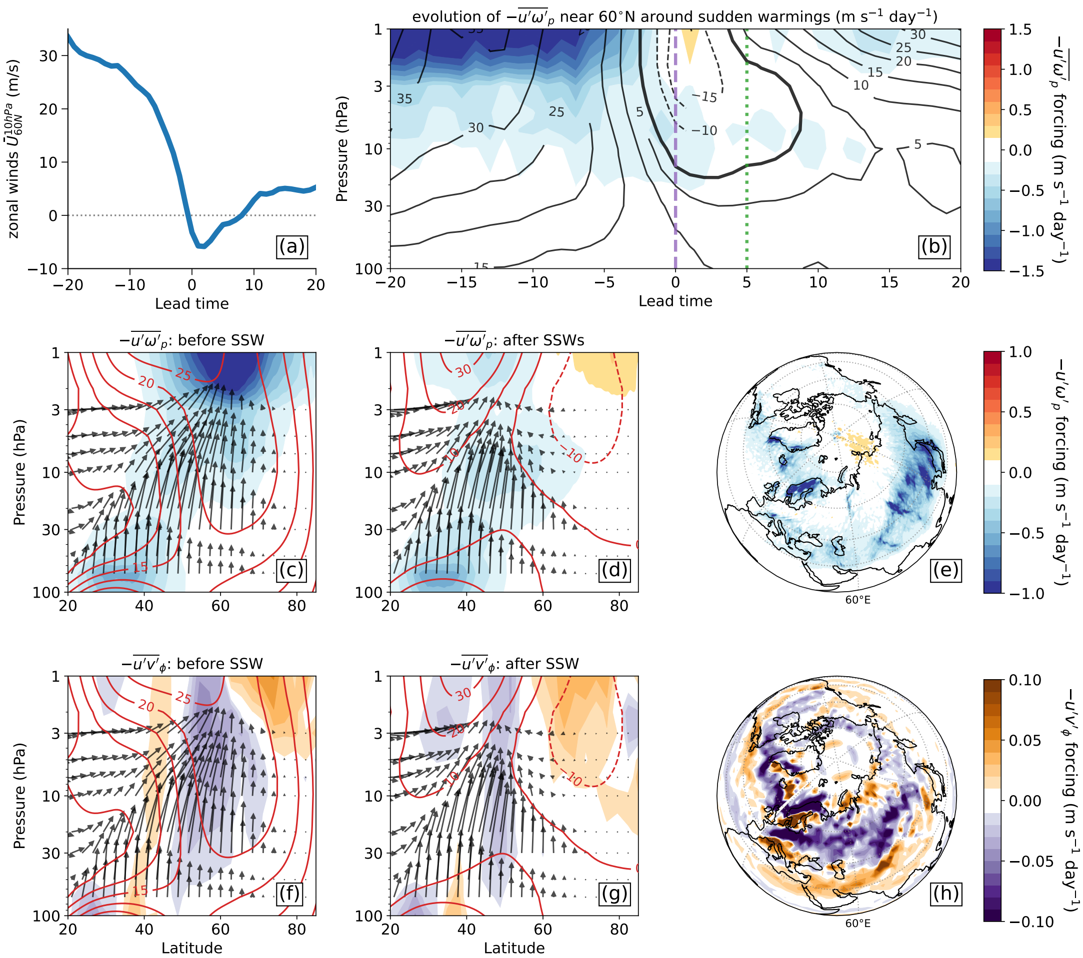

Figure 3. (a) Composite evolution of zonal mean zonal wind (m/s) at 60°N and 10 hPa around 30 major SSWs over 1979-2023 and (b) composite evolution of resolved GW forcing (m/s/day) due to vertical flux convergence, i.e. the $\overline{u'\omega'}_p$ term, at 60°N. (c) The latitude-pressure profile of the $\overline{u'\omega'}_p$ term before SSWs averaged over lead times -20 to 0 (to the left of violet bar in (b)), (d) the $\overline{u'\omega'}_p$ term shortly after SSWs averaged over lead times 0 to 5 (enclosed by violet and green bars in (b)). (e) The map of $-u'\omega'_p$ in the upper stratosphere (10 hPa) before SSWs, i.e., averaged over lead times -20 to 0. (f-h) Same as figures (c-e) respectively, but for the $\overline{u'v'}_\phi$ term. Black curves in (b) show the zonal mean zonal wind at 60°N. Red curves and black arrows in (c)-(d) and (f)-(h) respectively show the zonal mean zonal wind and small-scale EP-Flux.

A gradual reduction in -$\overline{u'\omega'}_p$ in the upper stratosphere is noticed 7-20 days before the event, followed by a dramatic reduction in the upper atmosphere GW forcing within 7 days of the warming (Figure 3b). Upon wind reversal, the deceleration happens at slightly lower altitudes (10-20 hPa). The reversal is also accompanied by a reversal in the GW forcing in the upper stratosphere, i.e., GW dissipation provides a net acceleration to the zonal mean flow, likely due to predominantly westward propagating GWs experiencing critical levels lower within the stratosphere.

The zonal wind below 10 hPa remains weak even 2-3 weeks after the SSW. Despite the zonal wind recovering to its original strength above 10 hPa, the GW forcing in the upper stratosphere remains weak relative to pre-warming strength. In the lower stratosphere, the GW forcing remains largely unaffected before and after the SSWs at all latitudes, contrasting the dramatic decrease in forcing in the upper stratosphere (Figure 3c vs. 3d). The decrease is accompanied by (a) an equatorward shift in the westward drag dissipation with wave focusing towards the new jet maximum at 30-35°N, and (b) GWs providing a net acceleration poleward of 60°N (Figure 3c vs. 3d).

The composite map of -$\overline{u'\omega'}_p$ before SSWs exhibits a wave-1 structure likely associated with wind anomalies around SSWs (Figure 3e); computing anomalies from the DJF climatologies reveal strengthening of the westward GW dissipation over the Central and East Asian mountains (Supplementary Figure S2). This seems consistent with the findings from the topography-removal experiments of White et al. (2018) that found these mountain ranges to strongly influence the Northern Hemisphere SSW frequency.

Changes in the $\overline{u'\omega'}_p$ term are accompanied by changes in the $\overline{u'v'}_\phi$ term. Before SSWs, lateral flux dissipation provides net deceleration in the jet-center region (Figure 3f; purple). Following SSWs, the equatorward shift in the jet leads to an equatorward shift in the lateral flux dissipation. Moreover, the dissipation provides a net acceleration in the region with polar easterly winds (Figure 3g). The map of $u'v'_\phi$ (Figure 3h) shows that most of the contribution to the midlatitude convergence (deceleration) noted in the zonal mean (in Figure 3f) occurs over Northern Atlantic, mainland Europe, and Northern Asia. Likewise, the divergence (acceleration) between 35-45°N occurs mostly over continental Asia, Middle East, and Southern Europe.

5.2 Evolution around Antarctic Final Warmings

We extend the analysis of Gupta et al. (2021) to assess lateral flux evolution around FWs.

Approaching the FW, strong westerlies in the extratropical winter stratosphere gradually weaken with an average deceleration of –1.2 m/s/day (Figure 4a). Composite evolution of the $\overline{u'\omega'}_p$ term around 60°S during this period shows a forcing of up to –3.5 m/s/day in the upper stratosphere. The GW deceleration in the upper stratosphere rapidly weakens 30-35 days before the FWs (Figure 4b color). The weakening is accompanied by a steady downward migration of the zero wind line and GW dissipation to lower altitudes. During this period, GWs from over a broad range of latitudes propagate upward and poleward and, on average, provide a peak resolved forcing of –1 m/s/day centered around 60-65°S (Figure 4c). Following the FW, the reversal in the mean winds leads to the filtering of all stationary and westward GWs in the lower-to-middle stratosphere. The eastward GWs propagating into the upper stratosphere and mesosphere provide a weak acceleration of the easterly winds (Figure 4d, red). A majority of the contribution to the zonal forcing by the $\overline{u'\omega'}_p$ term is due to waves excited over the Andes and the peninsula (Figure 4f). The fluxes from these waves, along with non-orographic waves from storm tracks (Hendricks et al., 2014; Holt et al., 2017) converge over the Southern Ocean around 60°S, providing a spiral belt of GW forcing. Near the Andes, the belt is centered around 55°S but around the Ross Sea (120°E) the belt center shifts to ∼65°S.

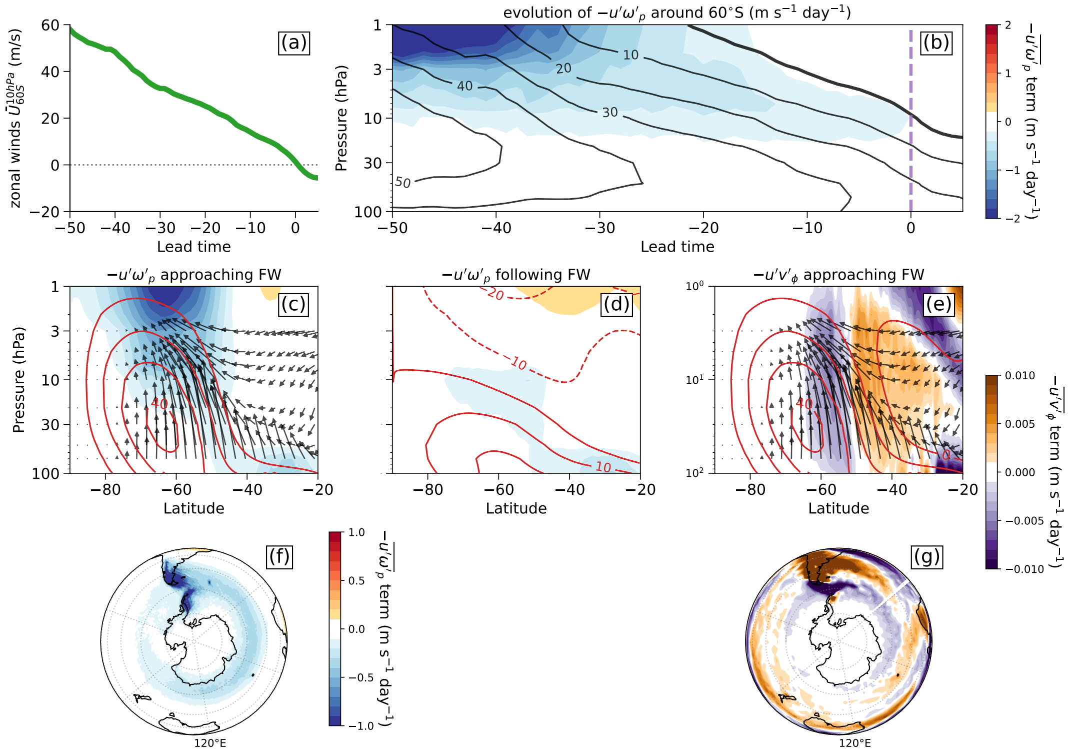

Figure 4. (a) Composite evolution of zonal mean zonal wind (m/s) at 60°S and 10 hPa around 44 FWs over 1979-2023, and (b) composite evolution of resolved GW forcing (m/s/day) from the $\overline{u'\omega'}_p$ term, at 60°S. (c) The latitude-pressure profile of the resolved forcing before FWs averaged over lead times -50 to 0 (left of the violet bar in (b)). (d) resolved GW forcing shortly after FWs averaged over lead times 0 to 5 (right of the violet bar in (b)). (e) The latitude-pressure profile of the forcing from lateral flux convergence, i.e. the $-\overline{u'v'}_\phi$ term averaged over lead times -50 to 0. (f)-(g) Map of the GW forcing from the $-\overline{u'\omega'}_p$ and $-\overline{u'v'}_\phi$ terms respectively averaged over lead times -50 to 0. Black curves in (b) show the zonal mean zonal wind at 60°S. Red curves and black arrows in (c)-(e) respectively show the zonal mean zonal wind and small-scale EP-Flux. (c), (d) and (f) share the same colorscale, so do (e) and (g).

Contrary to the JJA mean, the zonal mean forcing from the $\overline{u'v'}_\phi$ term around FWs is one-to-two orders of magnitude weaker than that from the $\overline{u'\omega'}_p$ term (Figure 4e vs 4c). This is because strong deceleration from this term is localized around the Andes and in the zonal mean is balanced by the acceleration provided by lateral fluxes over other sources around Southern Africa and Oceania (Figure 4g). Nevertheless, strong local deceleration from this term can be important for an accurate representation of mesoscale variability around the Drake Passage and over the Southern Ocean.

6 Conclusions and Discussion

We produce a 44-year DJF and JJA climatology of resolved zonal GW forcing in the extratropical stratosphere using ERA5 and assess its composite evolution around Boreal SSWs and Austral FWs. We analyze both the vertical and the meridional flux of GW pseudomomentum to quantify the impact of lateral propagation towards the zonal flow forcing. Model parameterizations of GWs typically ignore lateral effects and only focus on vertical propagation when approximating subgrid-scale fluxes. Relative forcing contribution from these terms demonstrates that lateral propagation effects are prominent in the midlatitudes, especially near orography, and could be important for the middle-to-upper stratospheric circulation.

The analysis complements other efforts to (i) produce GW climatology in the stratosphere using observations (Geller et al., 2013; Ern et al., 2018; Hindley et al., 2020; Wei et al., 2022, for instance), (ii) analyze GW contributions towards stratospheric circulation and variability (Polichtchouk et al., 2018; Sato & Hirano, 2019; Eichinger et al., 2020; Gupta et al., 2021; Cullens & Thurairajah, 2021; Pahlavan et al., 2021), and (iii) assess the complete GW forcing (Kruse et al., 2022; Procházková et al., 2023; Sun et al., 2023).

Following the Transformed Eulerian Mean framework, we estimate the mean GW pseudomomentum flux by estimating the vertical flux of zonal momentum ($u'\omega'$), meridional flux of zonal momentum ($u'v'$), and meridional heat flux ($v'\theta'$). The vertical convergence of $u'\omega'$ dominates the total GW forcing in both the DJF and JJA stratospheric midlatitudes, with the peak resolved JJA forcing at 40-45 km height (–4 m/s/day) being more than double in magnitude than the respective climatological DJF forcing (–1.5 m/s/day). Still, meridional convergence of lateral fluxes forms a considerable fraction of the forcing around orography and over the Southern Ocean, providing a zonal mean resolved forcing of –0.5 m/s/day at those altitudes.

The lateral effects in the Southern Hemisphere are stronger during peak winter than during springtime. Lateral propagation of GWs, together with local GW sources, leads to the formation of belts of GW activity in both hemispheres' upper stratosphere. Momentum flux hotspots appear over orography but appear to spread over a much broader region in the upper stratosphere due to lateral propagation.

The composite evolution of GW forcing around major SSWs and FWs demonstrates the sensitivity of GW forcing to changes in the stratospheric mean state, suggesting possible changes in stratospheric GW forcing in a changing climate. Abrupt changes to the polar vortex are associated with abrupt changes in the upper stratospheric GW forcing due to changes in GW propagation conditions. Even after the vortex recovers to pre-SSW strength in the upper stratosphere, persisting wind anomalies in the middle stratosphere prevent tropospheric GWs from propagating into the upper stratosphere.

The analysis only provides a glimpse into the true GW climatology, as ERA5 and even high-resolution models underestimate the resolved GW forcing in the stratosphere on account of prescribed dissipation or limited grid resolution (Holt et al., 2016; Wicker et al., 2023; Gupta et al., 2024). These unresolved GWs, with wavelength $\in (10, 100)$ km, can account for a major chunk of extratropical GW forcing (Polichtchouk et al., 2022, 2023). The stratospheric sponge in ERA5 between 1-10 hPa could also attenuate the resolved GWs. Further, computing vertical convergence on 37 pressure levels, as opposed to 137 model levels, likely underestimates the forcing. Lastly, Gaussian tapering of complex coefficients dampens the contributions from spatial scales 500-1000 km to some degree (Figure S3), resulting in weaker GW forcing profiles than those in previous studies which employ a fixed-wavenumber cutoff (Geller et al., 2013; Wicker et al., 2023; Gupta et al., 2021).

The findings affirm the importance of lateral propagation, suggesting its importance for GW parameterization development. Neglecting lateral propagation is believed to be a prime reason for "missing drag" around 60°S, causing temperature biases and delayed Antarctic vortex breakdown in climate models (Sato et al., 2012). In fact, in addition to GWs (Plougonven et al., 2020; Eichinger et al., 2023; Voelker et al., 2023), model representation of a multitude of mesoscale processes including tropical (slantwise) convection (Chen et al., 2018), planetary boundary layers (Xie et al., 2012), radiative transfer (Jakub & Mayer, 2017), and convective boundary layer (Sorbjan, 2009), could stand to benefit from a nonlocal (three-dimensional) parameterized representation.

Data Availability Statement

ECMWF's ERA5 data can be freely accessed from `https://www.ecmwf.int/en/forecasts/datasets/reanalysis-datasets/era5`

Acknowledgments

This research was made possible by Schmidt Futures, a philanthropic initiative founded by Eric and Wendy Schmidt, as part of the Virtual Earth System Research Institute (VESRI). AS acknowledges support from the National Science Foundation through grant OAC-2004492, and MJA acknowledges support from NSF grant OAC/CLD-2004512.

References

Achatz, U., Alexander, M. J., Becker, E., Chun, H.-Y., Dörnbrack, A., Holt, L., … Wright, C. J. (2023, November). Atmospheric Gravity Waves: Processes and Parameterization. *Journal of the Atmospheric Sciences*, *-1*(aop). doi: 10.1175/JAS-D-23-0210.1

Albers, J. R., & Birner, T. (2014, November). Vortex Preconditioning due to Planetary and Gravity Waves prior to Sudden Stratospheric Warmings. *J. Atmos. Sci.*, *71*(11), 4028–4054. doi: 10.1175/JAS-D-14-0026.1

Alexander, M. J., Geller, M., McLandress, C., Polavarapu, S., Preusse, P., Sassi, F., … Watanabe, S. (2010). Recent developments in gravity-wave effects in climate models and the global distribution of gravity-wave momentum flux from observations and models. *Quarterly Journal of the Royal Meteorological Society*, *136*(650), 1103–1124. doi: 10.1002/qj.637

Alexander, M. J., & Grimsdell, A. W. (2013). Seasonal cycle of orographic gravity wave occurrence above small islands in the Southern Hemisphere: Implications for effects on the general circulation. *Journal of Geophysical Research: Atmospheres*, *118*(20), 11,589–11,599. doi: 10.1002/2013JD020526

Andrews, D., Leovy, Conway, & Holton, James. (1987). *Middle Atmosphere Dynamics, Volume 40 - 1st Edition.*

Baldwin, M. P., Ayarzagüena, B., Birner, T., Butchart, N., Butler, A. H., Charlton-Perez, A. J., … Pedatella, N. M. (2021). Sudden Stratospheric Warmings. *Reviews of Geophysics*, *59*(1), e2020RG000708. doi: 10.1029/2020RG000708

Becker, E. (2012, June). Dynamical Control of the Middle Atmosphere. *Space Sci Rev*, *168*(1), 283–314. doi: 10.1007/s11214-011-9841-5

Butler, A. H., Sjoberg, J. P., Seidel, D. J., & Rosenlof, K. H. (2017, February). A sudden stratospheric warming compendium. *Earth System Science Data*, *9*(1), 63–76. doi: 10.5194/essd-9-63-2017

Chen, T.-C., Yau, M. K., & Kirshbaum, D. J. (2018, July). Assessment of Conditional Symmetric Instability from Global Reanalysis Data. *Journal of the Atmospheric Sciences*, *75*(7), 2425–2443. doi: 10.1175/JAS-D-17-0221.1

Cullens, C. Y., & Thurairajah, B. (2021, August). Gravity wave variations and contributions to stratospheric sudden warming using long-term ERA5 model output. *Journal of Atmospheric and Solar-Terrestrial Physics*, *219*, 105632. doi: 10.1016/j.jastp.2021.105632

Domeisen, D. I. V., & Butler, A. H. (2020, December). Stratospheric drivers of extreme events at the Earth's surface. *Commun Earth Environ*, *1*(1), 1–8. doi: 10.1038/s43247-020-00060-z

Eichinger, R., Garny, H., Šácha, P., Danker, J., Dietmüller, S., & Oberländer-Hayn, S. (2020, March). Effects of missing gravity waves on stratospheric dynamics; part 1: Climatology. *Clim Dyn*, *54*(5), 3165–3183. doi: 10.1007/s00382-020-05166-w

Eichinger, R., Rhode, S., Garny, H., Preusse, P., Pisoft, P., Kuchař, A., … Kern, B. (2023, October). Emulating lateral gravity wave propagation in a global chemistry–climate model (EMAC v2.55.2) through horizontal flux redistribution. *Geoscientific Model Development*, *16*(19), 5561–5583. doi: 10.5194/gmd-16-5561-2023

Ern, M., Trinh, Q. T., Preusse, P., Gille, J. C., Mlynczak, M. G., Russell III, J. M., & Riese, M. (2018, April). GRACILE: A comprehensive climatology of atmospheric gravity wave parameters based on satellite limb soundings. *Earth System Science Data*, *10*(2), 857–892. doi: 10.5194/essd-10-857-2018

Fritts, D. C., & Alexander, M. J. (2003). Gravity wave dynamics and effects in the middle atmosphere. *Reviews of Geophysics*, *41*(1). doi: 10.1029/2001RG000106

Geller, M. A., Alexander, M. J., Love, P. T., Bacmeister, J., Ern, M., Hertzog, A., ... Zhou, T. (2013, September). A Comparison between Gravity Wave Momentum Fluxes in Observations and Climate Models. *Journal of Climate*, *26*(17), 6383–6405. doi: 10.1175/JCLI-D-12-00545.1

Gill, A. (1982). *Atmosphere-Ocean Dynamics, Volume 30 - 1st Edition.* https://shop.elsevier.com/books/atmosphere-ocean-dynamics/gill/978-0-12-283522-3.

Giorgetta, M. A., Manzini, E., & Roeckner, E. (2002). Forcing of the quasi-biennial oscillation from a broad spectrum of atmospheric waves. *Geophysical Research Letters*, *29*(8), 86-1-86-4. doi: 10.1029/2002GL014756

Gupta, A., Birner, T., Dörnbrack, A., & Polichtchouk, I. (2021). Importance of Gravity Wave Forcing for Springtime Southern Polar Vortex Breakdown as Revealed by ERA5. *Geophysical Research Letters*, *48*(10), e2021GL092762. doi: 10.1029/2021GL092762

Gupta, A., Reichert, R., Dörnbrack, A., Garny, H., Eichinger, R., Polichtchouk, I., ... Birner, T. (2024, January). Estimates of Southern Hemispheric Gravity Wave Momentum Fluxes Across Observations, Reanalyses, and Kilometer-scale Numerical Weather Prediction Model. *Journal of the Atmospheric Sciences*, *-1*(aop). doi: 10.1175/JAS-D-23-0095.1

Hendricks, E. A., Doyle, J. D., Eckermann, S. D., Jiang, Q., & Reinecke, P. A. (2014, May). What Is the Source of the Stratospheric Gravity Wave Belt in Austral Winter? *Journal of Atmospheric Sciences*, *71*(5), 1583–1592. doi: 10.1175/JAS-D-13-0332.1

Hersbach, H., Bell, B., Berrisford, P., Hirahara, S., Horányi, A., Muñoz-Sabater, J., ... Thépaut, J.-N. (2020). The ERA5 global reanalysis. *Quarterly Journal of the Royal Meteorological Society*, *146*(730), 1999–2049. doi: 10.1002/qj.3803

Hindley, N. P., Wright, C. J., Hoffmann, L., Moffat-Griffin, T., & Mitchell, N. J. (2020). An 18-Year Climatology of Directional Stratospheric Gravity Wave Momentum Flux From 3-D Satellite Observations. *Geophysical Research Letters*, *47*(22), e2020GL089557. doi: 10.1029/2020GL089557

Holt, L. A., Alexander, M. J., Coy, L., Liu, C., Molod, A., Putman, W., & Pawson, S. (2017, July). An evaluation of gravity waves and gravity wave sources in the Southern Hemisphere in a 7 km global climate simulation. *Q J R Meteorol Soc*, *143*(707), 2481–2495. doi: 10.1002/qj.3101

Holt, L. A., Alexander, M. J., Coy, L., Molod, A., Putman, W., & Pawson, S. (2016, September). Tropical Waves and the Quasi-Biennial Oscillation in a 7-km Global Climate Simulation. *Journal of the Atmospheric Sciences*, *73*(9), 3771–3783. doi: 10.1175/JAS-D-15-0350.1

Holton, J. R. (1982, April). The Role of Gravity Wave Induced Drag and Diffusion in the Momentum Budget of the Mesosphere. *Journal of the Atmospheric Sciences*, *39*(4), 791–799. doi: 10.1175/1520-0469(1982)039⟨0791:TROGWI⟩2.0.CO;2

Jakub, F., & Mayer, B. (2017, November). The role of 1-D and 3-D radiative heating in the organization of shallow cumulus convection and the formation of cloud streets. *Atmospheric Chemistry and Physics*, *17*(21), 13317–13327. doi:

10.5194/acp-17-13317-2017

Kidston, J., Scaife, A. A., Hardiman, S. C., Mitchell, D. M., Butchart, N., Baldwin, M. P., & Gray, L. J. (2015, June). Stratospheric influence on tropospheric jet streams, storm tracks and surface weather. *Nature Geosci*, *8*(6), 433–440. doi: 10.1038/ngeo2424

Kim, Y.-J., Eckermann, S. D., & Chun, H.-Y. (2003, March). An overview of the past, present and future of gravity-wave drag parametrization for numerical climate and weather prediction models. *Atmosphere-Ocean*, *41*(1), 65–98. doi: 10.3137/ao.410105

Kruse, C. G., Alexander, M. J., Hoffmann, L., van Niekerk, A., Polichtchouk, I., Bacmeister, J. T., . . . Stein, O. (2022, April). Observed and Modeled Mountain Waves from the Surface to the Mesosphere near the Drake Passage. *Journal of the Atmospheric Sciences*, *79*(4), 909–932. doi: 10.1175/JAS-D-21-0252.1

Pahlavan, H. A., Fu, Q., Wallace, J. M., & Kiladis, G. N. (2021, March). Revisiting the Quasi-Biennial Oscillation as Seen in ERA5. Part I: Description and Momentum Budget. *Journal of the Atmospheric Sciences*, *78*(3), 673–691. doi: 10.1175/JAS-D-20-0248.1

Pahlavan, H. A., Wallace, J. M., & Fu, Q. (2023, February). Characteristics of Tropical Convective Gravity Waves Resolved by ERA5 Reanalysis. *Journal of the Atmospheric Sciences*, *80*(3), 777–795. doi: 10.1175/JAS-D-22-0057.1

Plougonven, R., de la Cámara, A., Hertzog, A., & Lott, F. (2020). How does knowledge of atmospheric gravity waves guide their parameterizations? *Quarterly Journal of the Royal Meteorological Society*, *146*(728), 1529–1543. doi: 10.1002/qj.3732

Plougonven, R., & Zhang, F. (2014). Internal gravity waves from atmospheric jets and fronts. *Reviews of Geophysics*, *52*(1), 33–76. doi: 10.1002/2012RG000419

Polichtchouk, I., & Scott, R. K. (2020). Spontaneous inertia-gravity wave emission from a nonlinear critical layer in the stratosphere. *Quarterly Journal of the Royal Meteorological Society*, *146*(728), 1516–1528. doi: 10.1002/qj.3750

Polichtchouk, I., Shepherd, T. G., Hogan, R. J., & Bechtold, P. (2018, May). Sensitivity of the Brewer–Dobson Circulation and Polar Vortex Variability to Parameterized Nonorographic Gravity Wave Drag in a High-Resolution Atmospheric Model. *Journal of Atmospheric Sciences*, *75*(5), 1525–1543. doi: 10.1175/JAS-D-17-0304.1

Polichtchouk, I., van Niekerk, A., & Wedi, N. (2023, January). Resolved Gravity Waves in the Extratropical Stratosphere: Effect of Horizontal Resolution Increase from O(10) to O(1) km. *Journal of the Atmospheric Sciences*, *80*(2), 473–486. doi: 10.1175/JAS-D-22-0138.1

Polichtchouk, I., Wedi, N., & Kim, Y.-H. (2022). Resolved gravity waves in the tropical stratosphere: Impact of horizontal resolution and deep convection parametrization. *Quarterly Journal of the Royal Meteorological Society*, *148*(742), 233–251. doi: 10.1002/qj.4202

Procházková, Z., Kruse, C. G., Alexander, M. J., Hoffmann, L., Bacmeister, J. T., Holt, L., . . . Šácha, P. (2023, June). Sensitivity of Mountain Wave Drag Estimates on Separation Methods and Proposed Improvements. *Journal of the Atmospheric Sciences*, *80*(7), 1661–1680. doi: 10.1175/JAS-D-22-0151.1

Sato, K., & Hirano, S. (2019, April). The climatology of the Brewer–Dobson circulation and the contribution of gravity waves. *Atmospheric Chemistry and Physics*, *19*(7), 4517–4539. doi: 10.5194/acp-19-4517-2019

Sato, K., Tateno, S., Watanabe, S., & Kawatani, Y. (2012, April). Gravity Wave Characteristics in the Southern Hemisphere Revealed by a High-Resolution Middle-Atmosphere General Circulation Model. *Journal of Atmospheric Sciences*, *69*(4), 1378–1396. doi: 10.1175/JAS-D-11-0101.1

Sato, K., Watanabe, S., Kawatani, Y., Tomikawa, Y., Miyazaki, K., & Takahashi,

M. (2009). On the origins of mesospheric gravity waves. *Geophysical Research Letters*, *36*(19). doi: 10.1029/2009GL039908

Song, B.-G., Chun, H.-Y., & Song, I.-S. (2020, September). Role of Gravity Waves in a Vortex-Split Sudden Stratospheric Warming in January 2009. *Journal of the Atmospheric Sciences*, *77*(10), 3321–3342. doi: 10.1175/JAS-D-20-0039.1

Sorbjan, Z. (2009, January). Improving Non-local Parameterization of the Convective Boundary Layer. *Boundary-Layer Meteorol*, *130*(1), 57–69. doi: 10.1007/s10546-008-9331-9

Sun, Y. Q., Hassanzadeh, P., Alexander, M. J., & Kruse, C. G. (2023). Quantifying 3D Gravity Wave Drag in a Library of Tropical Convection-Permitting Simulations for Data-Driven Parameterizations. *Journal of Advances in Modeling Earth Systems*, *15*(5), e2022MS003585. doi: 10.1029/2022MS003585

Voelker, G. S., Bölöni, G., Kim, Y.-H., Zängl, G., & Achatz, U. (2023, September). *MS-GWaM: A 3-dimensional transient gravity wave parametrization for atmospheric models* (No. arXiv:2309.11257). arXiv.

Wei, J., Zhang, F., Richter, J. H., Alexander, M. J., & Sun, Y. Q. (2022, October). Global Distributions of Tropospheric and Stratospheric Gravity Wave Momentum Fluxes Resolved by the 9-km ECMWF Experiments. *Journal of the Atmospheric Sciences*, *79*(10), 2621–2644. doi: 10.1175/JAS-D-21-0173.1

White, R. H., Battisti, D. S., & Sheshadri, A. (2018). Orography and the Boreal Winter Stratosphere: The Importance of the Mongolian Mountains. *Geophysical Research Letters*, *45*(4), 2088–2096. doi: 10.1002/2018GL077098

Wicker, W., Polichtchouk, I., & Domeisen, D. I. V. (2023, January). Increased vertical resolution in the stratosphere reveals role of gravity waves after sudden stratospheric warmings. *Weather and Climate Dynamics*, *4*(1), 81–93. doi: 10.5194/wcd-4-81-2023

Xie, B., Fung, J. C. H., Chan, A., & Lau, A. (2012). Evaluation of nonlocal and local planetary boundary layer schemes in the WRF model. *Journal of Geophysical Research: Atmospheres*, *117*(D12). doi: 10.1029/2011JD017080